https://doi.org/10.5194/egusphere-2024-2329
Preprint. Discussion started: 19 August 2024

Large-scale assessment of rainfall-induced landslide hazard based on hydrometeorological information: application to Partenio Massif (Italy)

Daniel Camilo Roman Quintero[1], Pasquale Marino[1], Abdullah Abdullah[1], Giovanni Francesco Santonastaso[1], Roberto Greco[1]
[1]Dipartimento di ingegneria, Università degli Studi della Campania "Luigi Vanvitelli", via Roma 9, Aversa (CE), 81038, Italy;
Correspondence to: Pasquale Marino (pasquale.marino1@unicampania.it)

Abstract. The definition of reliable tools for rainfall-induced landslide hazard assessment is often limited by the lack of long records of occurred landslides and relevant hydrometeorological variables. This is the case of the mountainous areas of Southern Apennines of Campania (Italy), diffusely covered by loose pyroclastic deposits laying upon limestone bedrock, and frequently subjected to rainfall-triggered shallow landslides. To get around this issue, a 500-year long synthetic dataset of the response to precipitation of a typical slope of the area has been generated, by means of a physically based model previously validated through experimental data. The obtained dataset, containing hourly values of soil moisture and suction, and of water level in an ephemeral aquifer developing in the uppermost fractured bedrock, has been used to assess slope stability through the calculation of the factor of safety. Based on the synthetic data, empirical thresholds for the prediction of landslide occurrence have been defined, either meteorological (i.e., based on rainfall intensity and duration) or hydrometeorological (i.e., coupling rainfall depth with antecedent root-zone soil moisture or aquifer water level). The results show that, where meteorological forcing and slope characteristics are perfectly known, hydrometeorological thresholds outperform the meteorological ones, and that a 3D threshold based on root-zone soil moisture, aquifer level, and rainfall depth, provides nearly unerring landslide predictions. The use of two antecedent hydrologic variables also allows identifying two different landslide triggering mechanisms, respectively typical of the beginning and of the end of the rainy season.

To extend the application to large areas, the uncertainties linked to the spatial variability on slope geomorphologic characteristics and hydrometeorological variables were considered as random errors. Hence, foreseeing the application to the north-facing side of Partenio Massif (about 80 km^2), the synthetic dataset has been perturbed, superimposing Normal-distributed random fluctuations to the calculated values of the factor of safety, and to the hydrometeorological variables used as landslide predictors. Although the uncertainty reduces the predictive skill of all the thresholds, the hydrometeorological ones show more robustness, with small numbers of both missed and false alarms. This result is confirmed by the application of the obtained thresholds to available data of landslides, rainfall and root-zone soil moisture for the period 2002-2020 in the area.

Keywords: Hydrometeorological thresholds; Early warning; Uncertainty analysis; Conditional landslide probability.

https://doi.org/10.5194/egusphere-2024-2329
Preprint. Discussion started: 19 August 2024

1 Introduction

Rainfall-induced landslides are a common natural hazard, involving the displacement of land portions in sloped areas following heavy rain periods. In urban zones, the effect of rainfall-induced landslides is critical due to human casualties, significant damages to man-made structures (e.g., roads and buildings), and substantial economic losses (Froude and Petley, 2018). Hence, predicting the occurrence of such kind of phenomena is highly relevant and needs to be deeply investigated.

Predicting rainfall-induced landslides often relies on defining empirical thresholds separating likely non-triggering from likely triggering conditions, which are key component of landslide early warning systems (LEWSs). The most common threshold is the purely meteorological relationship between rainfall intensity and duration (Guzzetti et al., 2007, 2008; Segoni et al., 2018). However, its lack of physical basis and its overconfidence in data correlations may give rise to important uncertainties, limiting the effectiveness of predictions.

It is well recognized that many rainfall-induced landslides are triggered on steep slopes covered with shallow granular deposits, usually in unsaturated conditions, following an increase in pore water pressure (Terzaghi, 1943), which is linked to an increase in the water stored in the soil (Bogaard and Greco, 2016). In the case of shallow landslides, the achievement of instability is favoured by antecedent wet soil conditions, thus landslide initiation depends not only on the triggering rainfall event characteristics (Mirus et al., 2018a; Wicki et al., 2020). More generally, the accumulation of water in a slope, up to the eventual triggering of a landslide, requires that slope drainage mechanisms are not capable of effectively draining out much of the infiltrating rainwater (Bogaard and Greco, 2016; Greco et al., 2021; Marino et al., 2021). Slope drainage processes are controlled by the hydraulic behaviour of the boundaries of the slope, which is often not static, as it may change in response to various large-scale processes (in time and space), which affect the slopes as parts of larger hydrological systems. The whole processes controlling slope infiltration and drainage represent the hydrologic predisposing factors (causes), which should be considered, together with rain event characteristics (trigger), in landslide prediction (Bogaard and Greco, 2018).

In the last decade, new advancements have been made in LEWS research. Novel hydrometeorological thresholds that combine hydrologic predisposing factors with rainfall events leading to slope failure have been developed for landslide forecasting. Specifically, adding hydrologic information physically linked to the predisposing processes occurring in the slope (e.g., soil moisture content) has been shown to improve the performance of LEWS from local/basin to regional scales (Abraham et al., 2021; Baum and Godt, 2010; Marino et al., 2020b; Mirus et al., 2018b; Palazzolo et al., 2023; Thomas et al., 2019). The acquisition of information about soil moisture is nowadays feasible, thanks to remote sensing (Beck et al., 2021), meteorological reanalysis products (Muñoz-Sabater et al., 2021), and through conventional field monitoring stations, at relatively low cost and in an up-to-date manner (Marino et al., 2020a, 2023). However, depending on site-specific characteristics, other hydrological variables as well as soil moisture may add valuable information to understand the seasonally changing slope response to precipitation (Illien et al., 2021; Roman Quintero et al., 2023).

Regardless the chosen approach (i.e., purely meteorological or hydrometeorological), a common issue in the definition of statistically significant empirical thresholds is the small number of unambiguously identified (in time and space) landslide

https://doi.org/10.5194/egusphere-2024-2329
Preprint. Discussion started: 19 August 2024

events in the historical records (Peres and Cancelliere, 2021), especially when the analysis is restricted to small areas (e.g., Gonzalez et al., 2023), such as single slopes or small catchments. Expanding the studied area (i.e., moving from local to regional landslide hazard assessment) allows increasing the number of valid landslide data, but it often implies encompassing quite different geomorphological and meteorological contexts in the same dataset, thus hampering the physical significance and reliability of the defined thresholds (Gonzalez et al., 2023; Segoni et al., 2018). One potential approach to address this issue is by defining landslide thresholds based only on non-triggering conditions, per definition much more numerous in any given dataset (Peres and Cancelliere, 2021). The dataset available for the definition of the threshold can also be enriched through the stochastic generation of synthetic data, an established technique in hydrology (e.g., Hanson, 1982; Michele et al., 2005; Salas et al., 2006; Keskin et al., 2006), and recently applied to landslide studies by coupling the stochastic generation of rainfall series with physically based infiltration and slope stability models (e.g., Peres and Cancelliere, 2014; Peres et al., 2018; Marino et al., 2021).

The case study of a relatively large landslide-prone area on the north-facing slopes of Partenio Massif (Campania, Southern Italy) is here analysed. The study area shares many major characteristics of landslide-affected areas in Campania: from a humid Mediterranean climate with densely vegetated slopes to soil deposits consisting of granular materials originating from the explosive eruptions of the Phleagrean Fields and the Somma-Vesuvius volcanoes (Rolandi et al., 1998). The shallow rainfall-induced landslides in the area always involve a mantle of a few meters of shallow air-fall pyroclastic deposits, mainly ashes with layers of pumices, overlaying a fractured karstic limestone bedrock, which during the rainy season hosts perched aquifers in its uppermost weathered part (epikarst) (Greco et al., 2018).

It is well-known that the triggering mechanism leading to rainfall-induced landslides on these slopes is the reduction of soil suction in the initially unsaturated deposits, and consequently of their shear strength, caused by soil wetting during rainwater infiltration (Damiano and Olivares, 2010; Olivares and Picarelli, 2003; Pagano et al., 2010; Pirone et al., 2015). Nevertheless, many features remain unknown in the application of this knowledge to wide areas especially for early warning purposes. As a matter of fact, heavy and persistent rainfall events are commonly followed by the triggering of landslides, but not all slopes (apparently similar) in relatively homogeneous geomorphological settings fail during the same event (Greco et al., 2021). In fact, the actual triggering of landslides depends on local geomorphologic slope features (Di Crescenzo and Santo, 2005; Crosta and Dal Negro, 2003), in some cases even affecting the mechanisms leading to slope failure, ranging from capillary barriers developing at the ash-pumice interface and causing flow diversion and local moisture accumulation (Reder et al., 2017), to locally impervious soil-bedrock interface impeding soil drainage and favouring pore pressure build-up (Damiano et al., 2012; Damiano and Olivares, 2010) to soil saturation caused by local exfiltration from the bedrock (Cascini et al., 2008).

This paper aims at defining empirical thresholds accounting for the effects of hydrometeorological and geomechanical spatial variability for operational use in a warning system for landslide forecasting in a wide area involving similar geomorphological settings. Two different approaches are compared for threshold definitions: a purely meteorological approach directly relating rainfall characteristics to landslide triggering, and a hydrometeorological approach based on a cause-trigger relationship. Both antecedent root-zone soil moisture and perched aquifer water level have been tested as possible proxies of hydrologic

https://doi.org/10.5194/egusphere-2024-2329
Preprint. Discussion started: 19 August 2024

predisposing conditions. To obtain a dataset rich enough for statistical analyses, rainfall stochastic generation is coupled with a physically based model of unsaturated flow and slope stability. Specifically, a 500-year long hourly synthetic dataset is used to capture the major hydrological processes occurring within the slope of Cervinara, belonging to north-facing slopes of Partenio Massif, and to assess slope stability. Initially, the analysis is conducted for a simplified reference slope model with a constant inclination, covered by a homogeneous soil layer with constant thickness. This approach provides a complete dataset including slope conditions (i.e., soil moisture, suction at various depths, and perched aquifer water level), allowing the assessment of the effects of every precipitation event on slope stability useful to define thresholds at the reference slope scale. As landslide triggering on real slopes in a wide area is influenced by local singularities, (e.g., related to spatial variability of soil properties, slope and bedrock morphology, soil cover thickness and layering, vegetation, and precipitation), random perturbations, generated with a Montecarlo technique, are introduced, to incorporate the effects of uncertainties referred to spatial variability of slope characteristics compared to the simplified reference slope model. The perturbed dataset mimics an operational early warning system covering the entire study area, based on monitoring information collected in few and sparse locations. To this aim, the effects of the spatial variability of monitored hydrometeorological variables (i.e., rainfall, soil moisture and aquifer level) have been also introduced as random fluctuations around the synthetic data.

The results show how, for the reference slope, perfectly described by the physically based model used for the generation of the synthetic dataset, it is possible to define a nearly unerring 3D hydrometeorological threshold coupling slope conditions one hour prior to the onset of rainfall events, expressed as the perched aquifer level and the root-zone soil moisture, with total event rainfall depth. The three hydrometeorological variables also allow identifying the antecedent conditions leading to two different landslide triggering mechanisms. For the same case, a 2D hydrometeorological threshold, based on soil moisture and rainfall depth, still ensures very high predictive performance (i.e., no missed alarms and about one false alarm every five years). The purely meteorological I-D threshold, instead, even in this perfectly known ideal operating condition, would lead to the unacceptable rate of one false alarm per year. The scale of application of the thresholds is enlarged to the entire north-facing side of the Partenio Massif, introducing the effects of the uncertainty related to spatial variability of hydrometeorological and geomorphological variables. The obtained results show the robustness of the hydrometeorological thresholds, compared to the purely meteorological one. In fact, the reduction of predictive performance at large scale results small, making the hydrometeorological thresholds still a reliable tool for landslide hazard assessment in the area, as confirmed by the application to the available landslide data of the period 2002-2020.

2 Materials and methods

2.1 Case study

The case study refers to an area of the Southern Apennines in Campania, Italy. Specifically, the studied slopes belong to the north-facing part of the Partenio Massif, about 40 km northeast of the city of Naples, with a total extension of about 80 km^2

https://doi.org/10.5194/egusphere-2024-2329
Preprint. Discussion started: 19 August 2024

(Fig. 1). They are covered by deposits of variable thickness of loose coarse-grained pyroclastic soil, consisting of alternating layers of ashes and pumices, lying upon a densely fractured limestone bedrock.

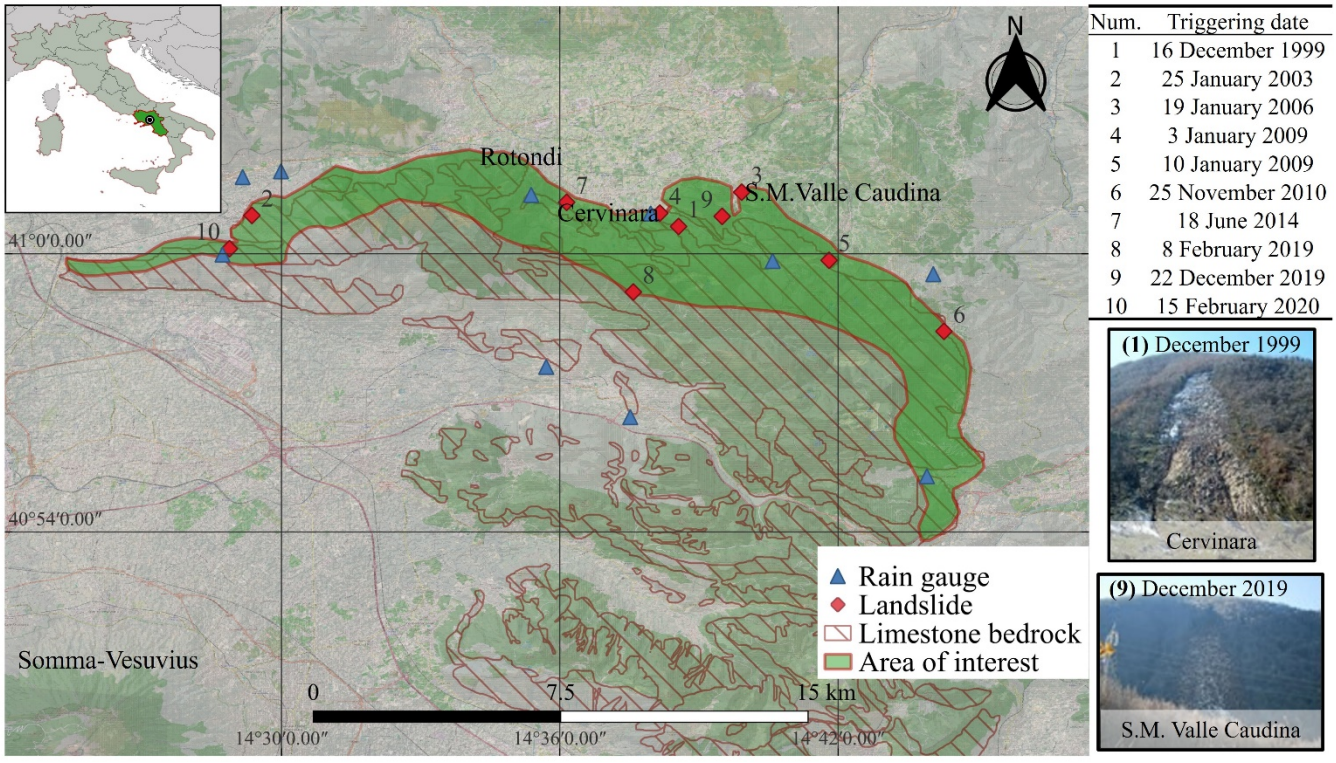

Figure 1. Study area of north-facing part of the Partenio Massif (green-filled area) with indication of the rain gauges and the major landslides reported in different landslide catalogues from 1999 to 2020 (sourced from: Peruccacci et al., 2023; Calvello and Pecoraro, 2018**).**

During the night between 15 and 16 December 1999, the slopes of Mt. Cornito (nearby the city of Cervinara) were affected by a series of shallow landslides after a rainfall event of about 320 mm in 48 hours. One of the major landslides travelled approximately 2 km from the source area and reached the town of Cervinara (Fiorillo et al., 2001), leaving human casualties and destroying buildings. Lately, in 2019, a huge debris avalanche affected the community of San Martino Valle Caudina (very close to Cervinara, Fig. 1), showing that this local area of a few km^2 belonging to northeast-facing slopes of Partenio Mountains is recurrently subjected to such kind of phenomena (Greco et al., 2021). The sliding surface of the previously described landslides, as well as in other similar geomorphological contexts of the region, usually occurs within the layers of ashes, a cohesionless soil characterized by friction angle values ranging between 37° and 39° (Olivares and Picarelli, 2003).

The fractured limestone formations are often the host rock for karstic aquifers. A distinction can be done between the weathered uppermost part of the bedrock, known as epikarst (Hartmann et al., 2014; Williams, 2008), more porous and pervious, and the deepest part, characterized by wider fracture systems, where the deep groundwater circulation is hosted. The interaction between the epikarst and the surface system is shown to be important for the hydrological behaviour of the unsaturated soil

https://doi.org/10.5194/egusphere-2024-2329
Preprint. Discussion started: 19 August 2024

cover (Roman Quintero et al., 2023). The water that leaks from the soil to the epikarst forms ephemeral perched shallow aquifers, that favour the recharge of the deep aquifer and supply surface water circulation through ephemeral springs.

2.2 Synthetic dataset of reference slope response to precipitation

A 500-year synthetic dataset was produced to mimic the major hydrological processes in the studied area. As is often the case with landslide studies, statistical analysis relying solely on historical observations would be limited by data scarcity. Hence, synthetic data generation is a suitable method to study slope hydrologic processes over a timescale long enough to allow for the occurrence of slope instability multiple times (e.g., Peres and Cancelliere, 2014; Peres et al., 2018; Marino et al., 2020b). The first step in generating a synthetic dataset is defining a reliable model of the major hydrological processes occurring within a slope, which will be used to assess slope stability. In this regard, a previously developed physically based model of unsaturated flow in the soil covering a simplified slope with known geometric, hydraulic, and geotechnical characteristics (referred to hereinafter as the reference slope model) was adopted. This model should be regarded as representative of the typical features of the slopes of the area. Although the soil cover is layered, effective parameters of a homogeneous soil layer resembling the mean hydraulic behaviour of the deposit have been assumed (Greco et al., 2013, 2018; Marino et al., 2020b). The model had been calibrated and validated according to field monitoring data and laboratory analyses, proving to be able to reliably reproduce field measurements (Comegna et al., 2016; Greco et al., 2013, 2014, 2018). As shown in Fig. 2, due to the relatively thin soil deposit in comparison to the length of the slope, the assumption of 1D flow is feasible. The interaction with the atmosphere considers rainfall infiltration and evapotranspiration, and the underlying perched aquifer, modelled as a linear reservoir, is connected to the overlying unsaturated soil through a coupling hydraulic condition assumed at the soil-bedrock interface.

https://doi.org/10.5194/egusphere-2024-2329
Preprint. Discussion started: 19 August 2024

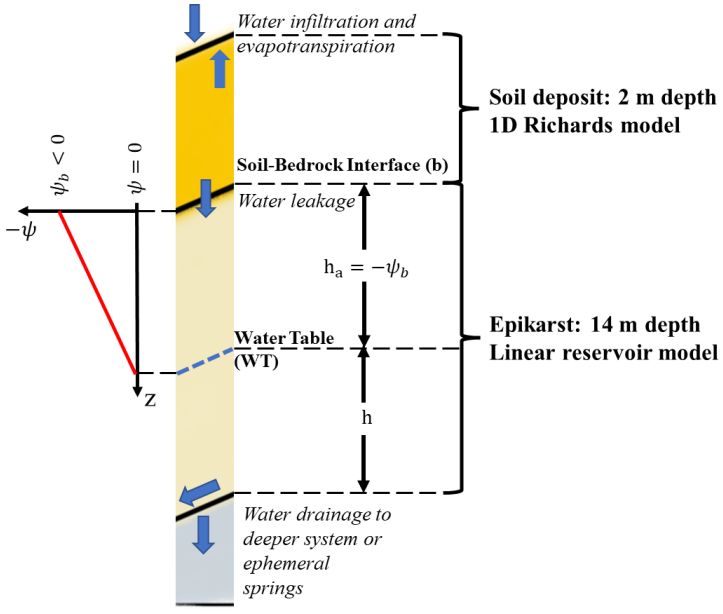

Figure 2. Water flow scheme for the 1D coupled flow model considering (from top to bottom): rainwater infiltration from the soil surface, unsaturated flow through the soil deposit accounting the effect of evapotranspiration, water leakage through the soil-bedrock interface, and saturated water flow in the epikarst joined to the soil-bedrock interface affecting the water potential.

The water flow in the unsaturated soil deposit is modelled assuming a homogeneous soil layer, using the 1D Richards' equation (1), where ψ is the soil matric potential, θ the volumetric water content, z is the vertical direction (see Fig. 2), and k is the unsaturated hydraulic conductivity. The actual evapotranspiration is considered in the source term q_r in Eq. (1), representing root water uptake, estimated from the potential evapotranspiration with the model of (Feddes et al., 1976), assuming a triangular root distribution penetrating the entire cover thickness.

$$\frac{\partial \theta}{\partial t} = \frac{dk}{d\theta}\frac{\partial \theta}{\partial z} + \frac{\partial}{\partial z}\left(k\frac{d\psi}{d\theta}\frac{\partial \theta}{\partial z}\right) - q_r \quad (1)$$

The hydraulic characteristic curves, $\theta(\psi)$ and $k(\psi)$, are modelled with the van Genuchten-Mualem model shown in Eqs. (2) and (3), where θ_r and θ_s are the residual and saturated volumetric water content, respectively; α, n, and $m = 1 - 1/n$ are shape parameters; $S_e = (\theta - \theta_r)/(\theta_s - \theta_r)$ is the effective degree of saturation; K_s is the saturated hydraulic conductivity (Mualem, 1976).

$$\theta(\psi) = \begin{cases} \theta_r + \dfrac{\theta_s - \theta_r}{(1 + \alpha|\psi|^n)^m} & \text{if } \psi < 0 \\ \theta_s \text{ if } \psi \geq 0 \end{cases} \quad (2)$$

$$k(\psi) = \begin{cases} K_s S_e^{0.5}\left[1 - \left(1 - S_e^{1/m}\right)^m\right]^2 & \text{if } \psi < 0 \\ K_s \text{ if } \psi \geq 0 \end{cases} \quad (3)$$

The unsaturated flow model in the soil cover is coupled with a linear reservoir model simulating the water accumulation in the epikarst aquifer. The water balance equation of the perched epikarst aquifer reads:

https://doi.org/10.5194/egusphere-2024-2329
Preprint. Discussion started: 19 August 2024

$$n_a \frac{dh}{dt} = i_b - \frac{\mathrm{h}}{K_a} \quad (4)$$

In Equation (4), n_a is epikarst effective porosity, h is the water table depth, i_b is the water leakage from the soil cover to the bedrock, and K_a is the time constant of the linear reservoir. The aquifer water level is assumed to linearly affect the suction (ψ_b) at the base of the soil deposit, $\psi_b = H_e - h$, where H_e is the epikarst thickness. All the model parameters are summarised in Table 1.

Table 1. Hydraulic parameters applied in the coupled model of 1D water flow for the unsaturated soil cover and for the perched aquifer hosted in the Epikarst.

Soil cover	$\boldsymbol{\theta_s}$ (-)	0.70
	θ_r (-)	0.01
	α (m^{-1})	6
	n (-)	1.3
	Soil cover thickness (m)	2
	Saturated hydraulic conductivity, K_s ($m \cdot s^{-1}$)	$3x10^{-5}$
	Slope inclination angle, β (°)	40
Epikarst	Epikarst thickness, H_e (m)	14
	Effective porosity (-)	0.005
	Time constant of linear reservoir (days)	871 days

The above-described model was run to simulate the water flow with a 500-year synthetic hourly rainfall series, generated with the Neyman-Scott Rectangular Pulse model (NSRP) (Rodriguez-Iturbe et al., 1987). The NSRP is a stochastic model that reproduces the rainfall process based on a random selection of the origin, rainfall amount and duration of single rainfall cells (rectangular pulses), that can overlap with each other. Specifically, every cell width and height represent the duration and the intensity of each rainfall cell, respectively. Hence, when many cells overlap, the total intensity at any time is the result of the direct summation of the intensities of the overlapping cells. The model has been calibrated with the method of moments (Cowpertwait et al., 1996; Peres and Cancelliere, 2014), based on a 17-year long rainfall dataset with a time resolution of 10 minutes, from the rain gauge of Cervinara, managed by the Civil Protection Agency of Campania (Marino et al., 2020b; Roman Quintero et al., 2023).

Equations (1) and (4) have been solved with the finite differences technique in a 2 cm spacing grid with hourly timestep, allowing to obtain the 500-year synthetic series of volumetric water content θ and water potential in the soil profile, and of perched aquifer water level in the epikarst (hereinafter it will be indicated as the depth of the water table below the soil-bedrock interface, $h_a = -\psi_b$, as sketched in Fig. 2).

Based on the results of the model simulations, slope stability is assessed by evaluating the factor of safety (FS) at every simulated time. The assumed 1D geometry allows carrying out the slope stability analysis under the infinite slope hypothesis, i.e., FS being the ratio between the resistive shear strength and the effective shear stress, derived from the equilibrium analysis of a soil column element of height d resting on a slope with inclination angle β:

https://doi.org/10.5194/egusphere-2024-2329
Preprint. Discussion started: 19 August 2024

$$FS = \frac{c' + \gamma d \cos^2 \beta \tan \phi' - \gamma_w S_e \psi \tan \phi'}{\gamma d \sin \beta \cos \beta} \quad (5)$$

In Equation (5), c' and ϕ' are effective soil cohesion and friction angle, respectively; γ_w is the unit weight of water; γ is the mean unit weight of the wet soil column; χ is the Bishop coefficient, function of ψ and here assumed equal to the effective degree of saturation ($\chi = S_e$) (Lu and Likos, 2006). As a layer of cohesive altered ashes is present near the soil-bedrock interface, with a typical thickness of about 50 cm, the failure depth is assumed at the base of the cohesionless soil profile, i.e., 1.5 m below the ground surface (Marino et al., 2021). Landslide triggering is assumed to occur whenever $FS < 1.0$.

Once the landslide triggering has been identified, an association between the rain events and the occurrence or non-occurrence of landslides is needed. To this aim, rainfall events have been separated within the 500-year hourly rainfall series, assuming that rainfall can be regarded as a new event only when the effects of the previous one have disappeared from the topsoil, the moisture of which controls rainwater infiltration during the new event. To this aim, a separation interval of 24 hours with rain depth smaller than the mean daily evapotranspiration, estimated as 2 mm/day, has been assumed, as after this time the topsoil moisture returned to the field capacity for all the simulated rainfall events (Roman Quintero et al., 2023). Under this assumption, 26363 rain events were identified, with durations between 1 and 427 h and total rainfall depth between 2 mm and 645 mm.

The way the rain events have been associated to the occurrence or non-occurrence of landslides is shown in Fig. 3.

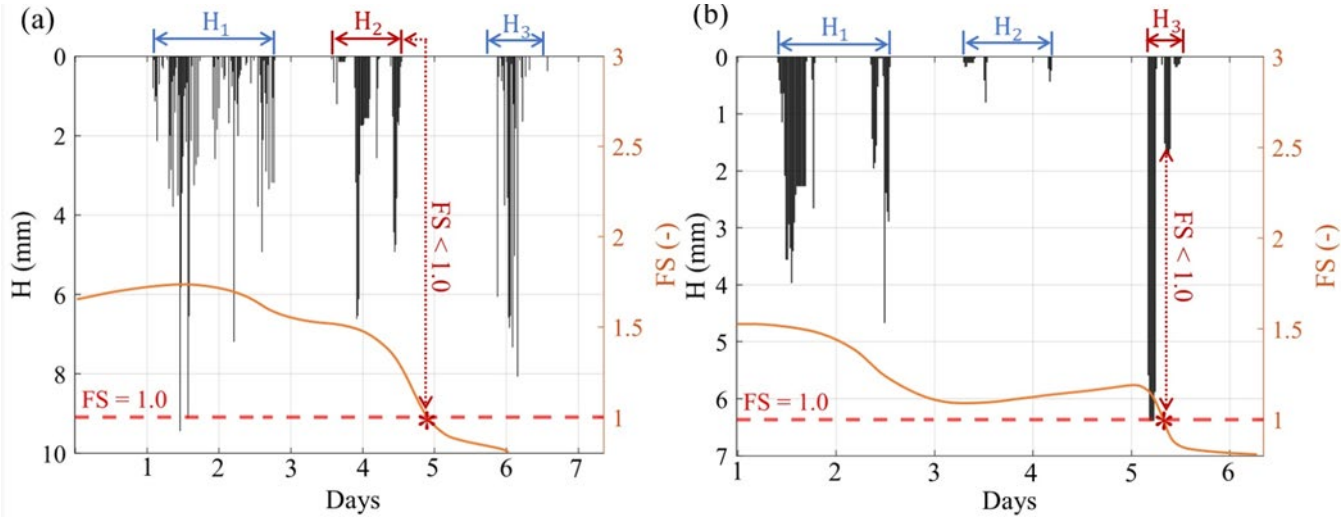

Figure 3. Schematic representation of the occurrence of landslides associated to rainfall events in two different cases: (a) associated to the previous event if FS < 1.0 after the end of the rainfall; (b) associated to the actual ongoing event if FS < 1.0 within the rainfall event.

Within the time series, the landslide occurrence condition (i.e., $FS < 1.0$) might be related to the triggering rain event in two different ways, as depicted in Figs. 5a and 5b, which show three rainfall events, H_1, H_2 and H_3. In the first case (Fig. 3a), $FS < 1.0$ is attained during a dry interval, owing to the delay in rainwater infiltration, thus the triggering of the landslide is associated to the previous rainfall event (H_2). In the second case (Fig. 3b), the critical condition is attained during the rainfall event H_3,

https://doi.org/10.5194/egusphere-2024-2329
Preprint. Discussion started: 19 August 2024

and so the landslide is associated to the ongoing event. To avoid misinterpretation of the actual triggering event, whenever the rainfall event associated to a landslide resulted smaller than 20 mm, it was merged with the immediately previous one.

2.3 Empirical landslide threshold definition

Empirical thresholds are a useful tool for separating rainfall events with landslides from those without. They consist in a line, or a surface, plotted in a suitable 2D or 3D space, often adopted in landslide early warning systems. The definition of empirical thresholds can be made with different functional formats, according to the shape of the data cloud in the chosen space (Mirus et al., 2024).

The hydrologic analysis of the synthetic dataset carried out by (Roman Quintero et al., 2023) has showed that, in the studied geomorphological context, the fraction of water remaining stored in the soil cover at the end of a rainfall event ($\Delta S/H$) is strongly related to the mean volumetric water content of the uppermost 100 cm of the soil profile (θ) and the antecedent perched aquifer water level (h_a), both evaluated one hour before the initiation of the event. This suggests that these two variables may be used for the definition of hydrometeorological landslide thresholds. Hence, different empirical thresholds have been here tested, aiming at comparing their landslide forecasting performances, ranging from the traditional meteorological rainfall intensity-duration threshold (D, I) to the hydrometeorological one (θ, H), in which the hydrological information θ has been considered as representative of conditions that predispose the slopes to failure, to novel functional format for hydrometeorological threshold defined in the 3D space (θ, h_a, H).

The parameters of all the tested functional formats for the empirical thresholds have been identified by maximizing the True Skill Statistic TSS (Peirce, 1884), which gives a measure of the predictive performance of the threshold:

$$\mathrm{TSS} = 1 - \frac{M}{P} - \frac{F}{N} \qquad (6)$$

In equation (6), M is the number of missed alarms (i.e., events not exceeding the threshold, but followed by a landslide), P is the total number of landslides (true positives), F is the number of false positives (i.e., rainfall events exceeding the threshold, without any landslide occurrence) and N is the total number of rainfall events not followed by any landslide (true negatives). A perfectly working threshold curve gives $\mathrm{TSS} = 1$, while $\mathrm{TSS} = -1$ indicates an always failing threshold. The objective function (6) is optimized by using a Genetic Algorithm (GA) (Goldberg and Holland, 1988).

Basically, it is worth to note that whenever $N \gg P$ (i.e., landslide triggering is a rare phenomenon), thus TSS is more sensitive to the missed alarms M, rather than to the false alarms F. Nevertheless, this bias can be useful for landslide prediction purposes, because a missed alarm error could have catastrophic consequences, while false alarms may only cause inconvenience to the served inhabitants and may affect their responsiveness and trust in an Early Warning System in the long run, owing to the well-known cry-wolf effect (Breznitz, 1984).

https://doi.org/10.5194/egusphere-2024-2329
Preprint. Discussion started: 19 August 2024

2.4 Real slope response to precipitation

The operational use of empirical thresholds for early warning purposes requires the monitoring (or prediction) of the adopted hydrometeorological variables, that are then used to identify the conditions leading to landslide occurrence. Compared to the simplified reference slope model, the real slopes of the study area present variable characteristics, in terms of geomorphology as well as hydraulic and mechanical properties of the soil. Spatial variability of slope characteristics, as well as of rainfall input, affects both the assessment of slope stability and the representativeness of the values of the variables used for the definition of the empirical threshold.

In this respect, to mimic the operational use of the empirical thresholds at large scale (i.e., referred to north-facing part of the Partenio Massif, about 80 km^2), the effects of the uncertainty affecting all the variables should be considered. Specifically, Normal distributed fluctuations are superimposed on the synthetic meteorological and hydrological variables used for the definition of the local thresholds.

2.4.1 Uncertainty in the hydrometeorological variables for threshold application to a large area

In the reference slope model, both the meteorological (i.e., rain event duration, depth, and mean intensity) and hydrological variables (i.e., root zone soil moisture and perched aquifer water level), that can be used for empirical thresholds definition, are perfectly representative of the actual meteorological forcing and hydrologic antecedent conditions of the slope. Instead, in real operational applications to a wide area, the same variables would be the result of sparse measurements or of model simulations with limited spatial resolution. Hence, the characteristics of the considered rainfall events are not those affecting all the slopes of the area. Similarly, the values of antecedent hydrological variables would not remain unchanged if measured (or simulated) at different points of the study area. Therefore, uncertainty affects the hydrometeorological variables to be used for threshold application to a large area. The greatness of uncertainty is related to the extension of the area to which the threshold is applied, compared to the spatial density of the input data.

For the case of the north-facing side of Partenio Mountains (about 80 km^2), the spatial variability of rain depth of events, separated as described in section 2.2, has been analyzed based on the experimental data recorded in the period 2001-2021 by three rain gauges managed by the Civil Protection in Cervinara, Rotondi, and San Martino Valle Caudina (S.M.V.C.), reported in Fig. 1. The distance between the rain gauges ranges from 4.8 km (between Rotondi and Cervinara) to 10.0 km (between Rotondi and S.M.V.C.), with the rain gauge of S.M.V.C. installed at a significantly higher altitude compared to the other two (Table 2). The rain events observed at different rain gauges, that overlapped for at least one hour in the time series, were considered contemporary. When the different intermittency of the rain observed at two gauges gave rise to the correspondence of a single event at a rain gauge with multiple shorter events at another, the short events were merged in a single event, so to obtain comparable total rainfall depths (i.e., in these cases, the separation criterion of 24 hours with less than 2 mm was disapplied). Table 2 reports some statistical indices of the difference of the rainfall observed at the three gauges, including the total number of events at each rain gauge, and the number of events overlapping with any of the others.

https://doi.org/10.5194/egusphere-2024-2329
Preprint. Discussion started: 19 August 2024

Table 2. Characteristics and degree of overlapping of rainfall events recorded at the three rain gauges of the study area.

Rain gauge	Elevation (m s.l.m.)	Mean yearly rainfall (mm)	Minimum and maximum event depth (mm)	Minimum and maximum event duration (h)	Total number of events	Number of events overlapping with Cervinara	Number of events overlapping with Rotondi	Number of events overlapping with S.M.V.C.
Cervinara	349	1600	[2, 266.6]	[1, 219]	1010	1010	845	831
Rotondi	483	1500	[2, 260.6]	[1, 218]	1010	845	1010	840
S.M.V.C.	850	2000	[2, 403]	[1, 290]	1052	831	840	1052

As an example, for two couplings of rain gauges, i.e. Cervinara with Rotondi and Cervinara with San Martino Valle Caudina, the scatterplots of the differences, $\Delta H = H_1 - H_2$, vs. the mean values, $H_{med} = (H_1 + H_2)/2$, of event depths recorded at the two gauges are reported in Fig. 4. The coupling between Rotondi and San Martino Valle Caudina has not been represented, as it resulted very similar to that of Cervinara with San Martino Valle Caudina.

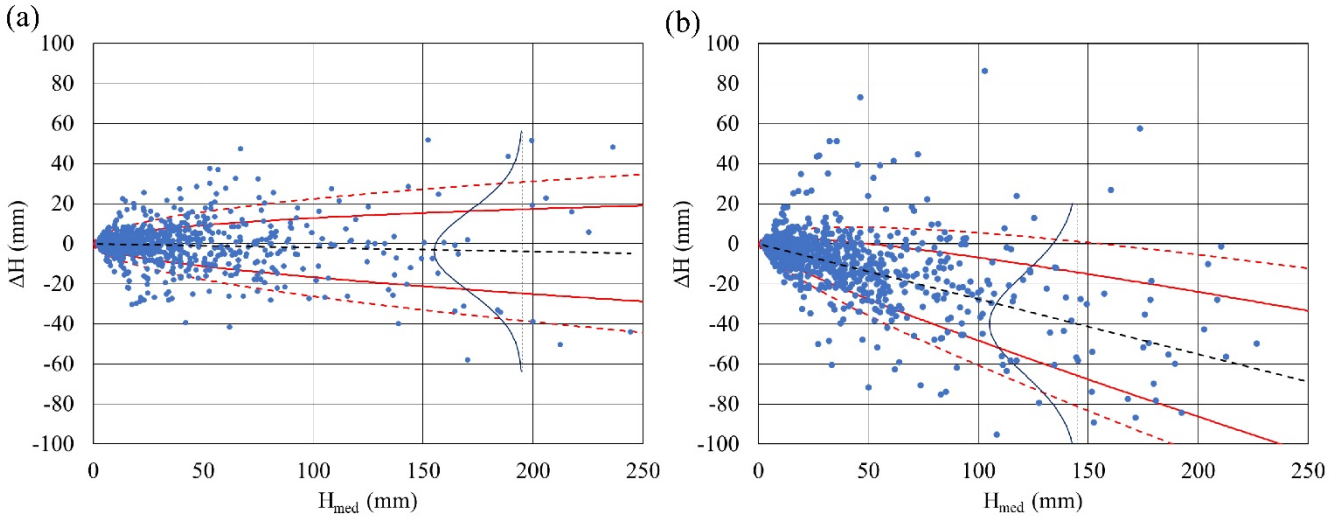

Figure 4. Scatterplots of the differences ΔH vs. the mean values H_{med} of rainfall depths of events recorded at the rain gauges of (a) Cervinara and Rotondi, and (b) Cervinara and San Martino Valle Caudina. The black dashed line represents the linear fitting of the $\Delta H(H_{med})$ relationship. The solid and dashed red lines are power-law equations around the black dashed line, including 68.3% and 86.6% of the dots, respectively.

The black dashed line in each graph represents the linear fitting of the dependence of the fluctuation ΔH on H_{med}, i.e., $\Delta H = \alpha H_{med}$. The solid and dashed red lines, symmetric around the black dotted line, represent equations of the format $\Delta H = \alpha H_{med} \pm A \times H_{med}^{B}$, with the power-law terms characterized by the same exponent B and different values of the coefficient A. The exponent B and the coefficients A of the solid and dashed curves, reported in table 3, have been obtained by searching the curves delimiting the zones containing 68.3% and 86.6% of the dots, respectively, and leaving outside the same number of

https://doi.org/10.5194/egusphere-2024-2329
Preprint. Discussion started: 19 August 2024

dots above and below them. If the ratio of the coefficients A obtained for the dashed and solid lines is close to 1.5, this indicates that the dot clouds are arranged in such a way to allow assuming the fluctuations of the rain depth difference to be Normal distributed around their mean, with mean and standard deviations depending on the mean total event depth according to the above mentioned linear and power-law relationships, respectively.

Table 3. Dependence of mean and standard deviation of rain event total depth fluctuations on mean total depth, for coupled rain gauge stations of the north side of Partenio mountains.

First rain gauge (H_1)	Second rain gauge (H_2)	α	A (68.3%)	A (86.6%)	B
Cervinara	Rotondi	-0.020	1.30	2.15	0.53
Cervinara	San Martino Valle Caudina	-0.276	1.38	2.21	0.59

The analysis of rain events for the three considered stations shows that both the distance and the difference of altitude affect the spatial variability of rainfall depth. Specifically, the rain event depths recorded at the stations of Rotondi and Cervinara, located at the foot of the north-facing slopes at close altitude, share the same mean, and the spreading of the depth difference around the mean looks similar. Whereas the rain gauge of San Martino Valle Caudina, at a significantly higher altitude, is considered, the dependence of mean event rain depth on the altitude clearly arises, and the spreading of rain depth difference looks slightly larger, as if the difference of elevation also affects event depth fluctuations and not only their mean value. However, the analysis of how topographic factors affect the spatial variability of rainfall event depth in the Partenio Massif cannot be based on the analysis of only three gauges, but it should be more deeply investigated based on rain data from all the rain gauges operating in the study area.

Regarding the variability of rain event depth moving away from the gauge position, the analyses for the three considered rain gauges indicates that the standard deviation of rain event depth at about 5 km from the measurement point can be approximated as $\sigma(H) \cong 1.5 \times H^{0.5}$. However, the density of the rain gauges managed by the Civil Protection agency in the study area (Fig. 1) is such that each rain gauge covers an area of about 10 km^2, so that the maximum distance of a slope from the closest rain gauge can be considered smaller than 2 km. Hence, to introduce the uncertainty deriving from the spatial variability of rain, the following relationship has been assumed for the standard deviation of rain event depth:

$$\sigma(H) = 0.75 \times H^{0.5} \quad (7)$$

Moreover, the uncertainty on the hydrological variables θ and h_a was introduced by considering a Normal-distributed random Absolute Error (AE) with zero mean and known standard deviation. Firstly, in the case of θ, the standard deviation of the AE distribution was assumed to be equal to 0.02. Brocca et al. (2012) showed that in relatively small areas (i.e. less than 100 km^2) monitored through conventional stations, an AE of $\pm$ 0.04 on the readings of θ can be addressed with a 95% confidence with a relatively low sampling density. Figure 5a shows the distribution of the AE on θ, where the 95% of the data falls between approximately $\pm$ 0.04. Similarly, (Dari et al., 2019) estimated that an AE in an area of about 500 km^2 instrumented with 12 stations shall be capable of give lectures with an error around 0.03, somehow confirming this picture even for larger areas. However, measurements obtained through remote sensing techniques, such as ERA-5 land products, often display a typical

https://doi.org/10.5194/egusphere-2024-2329
Preprint. Discussion started: 19 August 2024

error around 0.02 in the studied area (Hersbach et al., 2020; Muñoz-Sabater et al., 2021). Thus, the selected standard deviation of 0.02 encompasses the expected variability in volumetric water content measurements across different methodologies and environmental conditions.

Likewise, the standard deviation of the distribution of AE accounting for the uncertainty in the ground water monitoring, was assumed here to be equal to 1 m. Figure 5b presents the assumed distribution of AE on h_a, ranging around $\pm$2 m with a 95% confidence level. With this assumptions, the perturbed water levels will very unlikely approach the ground surface, consistently with the gushing out of water in natural springs at ground, observed rarely in the area, and only downhill, near the main streams Cornito and Castello (Marino et al., 2020b; Roman Quintero et al., 2023). The aim of introducing h_a is to assess the potential use of ephemeral aquifer formation in slope areas as an indicator of the conditions affecting water accumulation in the soil cover, including active and impeded drainage mechanisms (Roman Quintero et al., 2023). Indeed, some studies indicate that ephemeral aquifer systems can emerge in highlands and their water levels, related to wet and dry seasons, are spatially stable in wide areas (e.g., Bennett et al., 2022). In this respect, some data provided by one-year observations from wells placed downhill in the study area, show that the groundwater table depth difference at the wells seems to agree with the assumed maximum AE, ranging around $\pm$ 2 m (Autorità di Bacino, 2013).

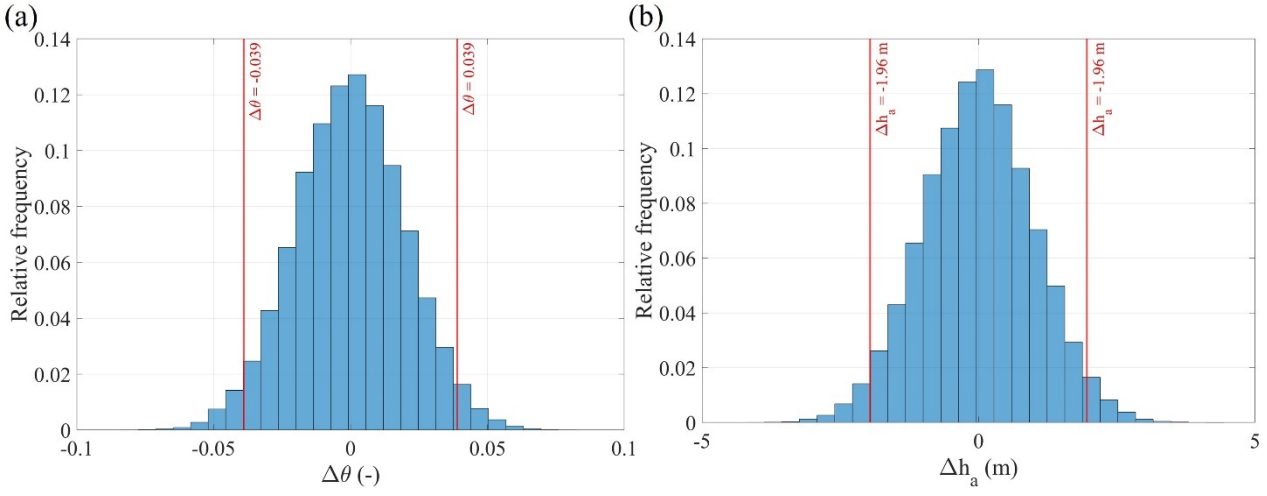

Figure 5. Frequency distributions of the absolute error associated with (a) the volumetric water content, $\Delta\theta$, and (b) the ground water level, Δh_a, assumed to randomly perturb the original dataset.

2.4.2 Uncertainty in the assessment of slope stability

In equation (5), the uncertainty of failure surface depth, d, and of slope inclination, β, depend on the variability of slope morphology; uncertainty of soil strength parameters, $c'$and ϕ', is linked to the variability of soil properties; uncertainty of soil column mean unit weight, γ, and of the value of ψ at the considered depth, may depend on the variability of both slope morphology and soil properties, as well as on the spatial variability of the meteorological forcing (mainly rainfall), vegetation

https://doi.org/10.5194/egusphere-2024-2329
Preprint. Discussion started: 19 August 2024

and boundary conditions. Hence, the uncertainty affecting the calculated values of FS has been assessed as the combined effects of all these uncertain factors, characterized as Normally distributed, with the standard deviations given in Table 4.

Table 4. Mean values and standard deviations of the factors affecting the uncertainty of the values of the factor of safety calculated for the simplified slope model.

Variable	Mean value (reference slope)	Standard deviation (Large scale)
$\boldsymbol{d}$ (m)	1.5	0.1
$\boldsymbol{\beta}$ (°)	40.0	2.0
$\boldsymbol{c'}$ (N/m^2)	0.0	0.0 (always assumed cohesionless soil)
$\boldsymbol{\phi'}$ (°)	38.0	0.5
$\boldsymbol{\gamma}$ (N/m^3)	variable for every event, depending on calculated soil moisture profile	10% of the mean
$\boldsymbol{\psi}$ (N/m^2)	variable for every event, depending on calculated FS value	1000.0
FS (-)	variable for every time	0.1

The values of the standard deviations reported in Table 4 for the large scale can be considered representative of the spatial variability of the characteristics of the slopes affected by shallow landslides in the north-facing side of Partenio Mountains (Fig. 1). In fact, the pyroclastic soil deposits, originated by the same eruptions, share similar stratigraphy and physical properties (e.g., Roman Quintero et al., 2024), thus explaining the small uncertainty affecting ϕ' and c'(this latter has been considered constantly equal to zero, as this is a conservative assumption for slope stability assessment). The factors related to slope morphology also present limited variability in the study area, as relatively big landslides usually occur in a relatively narrow range of inclination angles. In fact, slopes above 45° inclination typically present a very thin soil coverage (Del Soldato et al., 2018; De Vita and Nappi, 2013), while those with inclinations smaller than 35°, due to the high effective friction angle, would fail only if positive pore water pressure is reached. However, soil saturation is very unlikely in the considered slopes, thanks to the high porosity and hydraulic conductivity of the soil, as well as to the perviousness of the underlying fractured bedrock. Thus, the standard deviation of the fluctuation of FS around the values calculated for the simplified slope model results 0.10 (Table 4).

3 Results and discussion

3.1 Simplified reference slope thresholds

The slope stability analysis applied to the synthetic dataset of the reference slope leads to 20 triggering events in 500 years, a frequency which appears consistent with the historical dataset of landslides occurred nearby the city of Cervinara (landslides 1 and 9 of Fig. 1).

In Fig. 6, the scatterplots of triggering (red points) and non-triggering (green points) rainfall events are shown in the plane of rainfall duration and intensity (D, I), as well as in the plane of mean volumetric water content of the uppermost 100 cm and the rainfall events height (θ, H). The definition of the meteorological (Fig. 6a) and hydrometeorological (Fig. 6b) thresholds

https://doi.org/10.5194/egusphere-2024-2329
Preprint. Discussion started: 19 August 2024

have been made by means of power-law ($I = a\ D^b$) and linear ($H = a\theta + b$) functional formats, which share the same number of parameters.

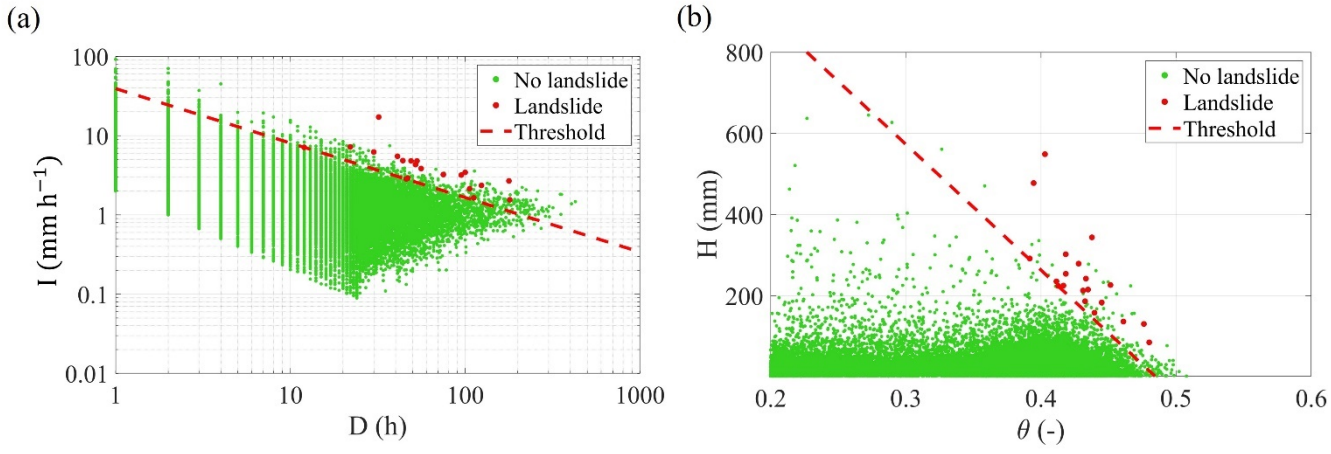

Figure 6. Power-law meteorological threshold (a); linear hydrometeorological threshold (b). In the 500 year-long synthetic data set, the red dots represent the rainfall events followed by the triggering of a landslide; the green ones are rainfall events after which no landslide occurs.

Table 5 summarizes the obtained parameters and the performance metrics for the tested thresholds.

Table 5. Parameters and metrics of the tested functional formats both the meteorological and hydrometeorological thresholds defined in Fig. 6.

Functional formats	a	b	TSS	Missed Alarms	False Alarms	Total events
Meteorological Power-law (Fig. 6a)	39.22	-0.69	0.983	0	452	26363
Hydrometeorological Linear (Fig. 6b)	-3097.86	1502.76	0.996	0	96	

As can be seen in Fig. 6a, the meteorological threshold captures the landslides occurring within rain intensities and durations ranging in several orders of magnitude. Instead, as shown in Fig. 6b, the adoption of a physically based hydrometeorological relationship can capture the extreme value nature of the landslide events, restricting the hazardous conditions to the outermost part of the dot cloud. In fact, most of the landslide red dots are disposed on the top-right side, where the soil wettest conditions occur and, sometimes, the highest rainfall events are also present. Since the separation between red and green points is well captured by the proposed hydrometeorological linear threshold, it performs better compared to the purely meteorological one (Table 5), even if both functional formats have the same number of parameters.

https://doi.org/10.5194/egusphere-2024-2329
Preprint. Discussion started: 19 August 2024

Moreover, the addition of a second hydrological variable (h_a) has allowed to incorporate the influence of the lowermost boundary condition of the soil cover, as seen in Fig. 7. Specifically, a novel 3D threshold format, consisting of two planes (θ, H) parallel to the axis h_a and separated by a limit value of perched aquifer water level (h_x), is proposed. In particular, the bi-plane format has 5 parameters: slope and intercept of the two traces of planes in the coordinate plane (θ, H), and the separating value of antecedent condition h_x, separating low from high water level (i.e., $H = a_1\theta + b_1$ with $h_a \geq h_x$ and $H = a_2\theta + b_2$ with $h_a < h_x$, respectively, Fig. 7b and Fig. 7c).

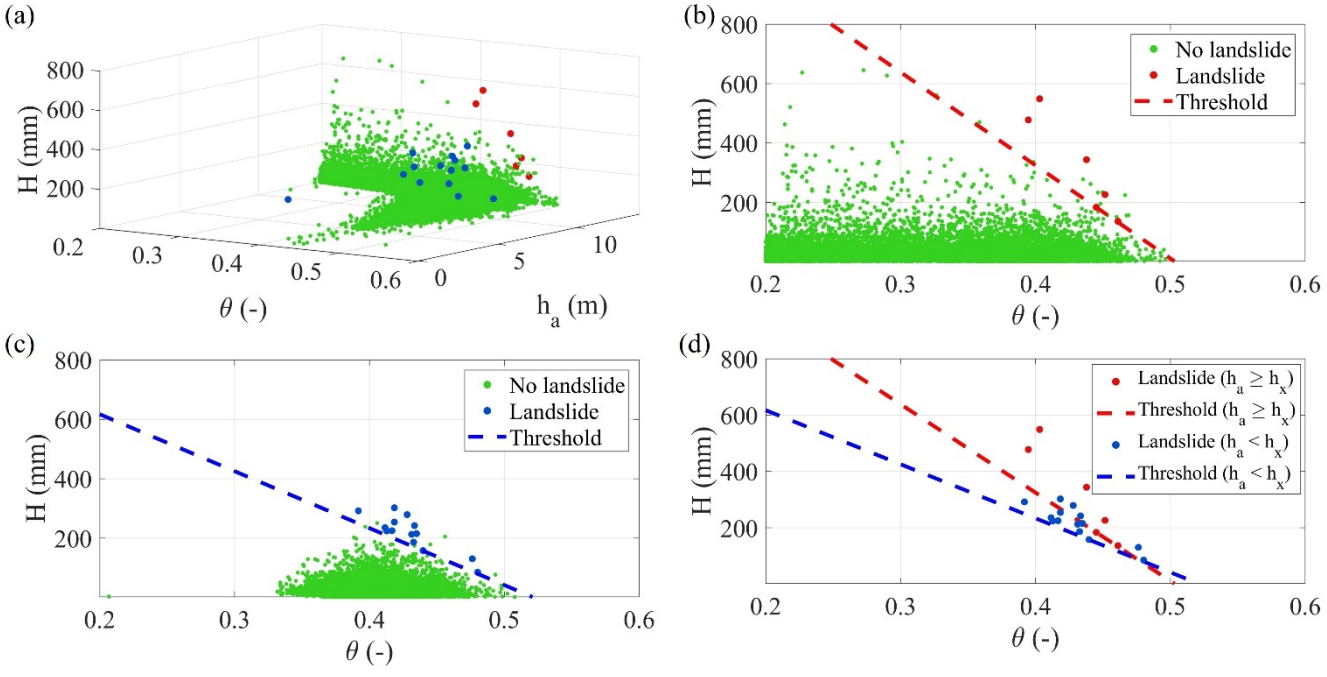

Figure 7. Optimal hydro-meteorological threshold in the space (θ, h_a, H): (a) scatter plot of data in the 3D space; (b) $h_a \geq 12.4$ m (low perched aquifer water level) and (c) $h_a < 12.4$ m (high perched aquifer water level). The green dots indicate conditions not leading to landslides. Landslide events have been split in red and blue dots, corresponding to different antecedent aquifer level; (d) comparison of the obtained thresholds for low and high aquifer level.

All the parameter values and the performance metrics obtained by maximization of TSS are reported in Table 6.

Table 6. Parameters of the tested functional format for the 3D hydrometeorological threshold defined in Fig. 7.

Functional format	Antecedent conditions	a	b	h_x	TSS	Missed alarms	False alarms	Total events
Bi-plane	$h_a \geq h_x$	-3134.03	1578.39	12.39	0.999	0	18	26363
	$h_a < h_x$	-1916.91	1000.42					

It is worth to note from Table 6 that the performance of this threshold is further improved compared to those obtained with 2D analysis (Table 5), leading to the lowest total number of false alarms, i.e., 18 in 500 years. The obtained value h_x (corresponding to about 12.4 m) provides the optimal separation between two triggering mechanisms. More specifically,

https://doi.org/10.5194/egusphere-2024-2329
Preprint. Discussion started: 19 August 2024

looking at Fig. 7b, the red dots represent landslides occurring with low perched aquifer water level (i.e., $h_a \geq h_x$), a condition typical of late autumn, which indicates that leakage through the soil-bedrock interface is hampered by the dryness of the lowermost part of the soil cover. In this condition, during large rainfall events, all the infiltrating water remains stored in the soil mantle, which is saturated from the top. Looking at Fig. 7c, instead, the blue dots represent landslides occurring with high epikarst aquifer water level ($h_a < h_x$), i.e., when the bedrock is already filled with the water previously leaked from the soil deposit, as observed after persistent rainy seasons. In this case, pore pressure increase occurs at the base of the soil deposit, which is saturated from the bottom, and in some cases even exfiltration from the bedrock can occur.

3.2 Large scale application

In operational applications of landslide forecasting in large areas, such as the Partenio Mountains, a simple tool for hazard assessment should be defined, relying on hydrometeorological information, typically available in few and sometimes sparse positions (i.e., the nodes of the grid of modelling or remote sensing products, or the locations of measurement instruments in the field). Therefore, the effects of spatial variability on slope stability as well on the representativeness of hydrometeorological information should be considered.

To this aim, the series of FS has been perturbed with Normal-distributed random fluctuations, with standard deviation 0.10 (section 2.4.2). Interestingly, 175 slope failures in 500 years have been obtained, corresponding to a mean frequency of more than one landslide every two years, which is comparable with the 10 landsides reported in the entire study area in the period 1999-2020 according to existing landslide catalogs (Calvello and Pecoraro, 2018; Peruccacci et al., 2023).

Similarly, the spatial variability of the hydrometeorological variables (θ, h_a, H), used for the definition of the threshold for the reference slope (section 3.1) and supposed to be measured in a single place for the considered area, has been introduced. Specifically, 100 different perturbed series (hereinafter "scenarios") have been generated embedding both the hydrological (θ and h_a) and meteorological (H) information as probabilistic variables with Normal-distributed random fluctuations with zero mean and the standard deviation values reported in section 2.4.1. For the sake of simplicity, the duration of rainfall events has been left unchanged, and the perturbed mean intensity has been obtained as $I = HD^{-1}$.

For all the scenarios, Fig. 8 shows the scatter plots of the perturbed variables in the planes (D, I) and (θ, H). The red dots represent the conditions followed by landslide occurrence, the green dots those without landslides. It looks clear from the dot arrangement that, even considering the randomness due to the spatial variability of all the considered variables, the hydrometeorological variables θ and H separate landslides from non-landslides much more effectively than the meteorological variables I and D. This result is confirmed by the landslide probability distributions, reported in Fig. 9 in the same planes. To draw the graphs, a rectangular grid with variable spacing has been defined, so to have at least 20 dots falling within each rectangle. The landslide probability has been estimated in each rectangle as the ratio between the number of landslides and the total number of dots. Indeed, the transition from small to high probability of landslide looks sharper in the (θ, H) plane than in the (D, I) plane (notice that this latter graph is plotted in logarithmic scales). This suggests that the adoption of a threshold line to separate landslides from non-landslides, as an operational tool for landslide hazard assessment, should ensure a good

https://doi.org/10.5194/egusphere-2024-2329
Preprint. Discussion started: 19 August 2024

performance in the (θ, H) plane, containing at the same time both missed and false alarms. The shape of the transition zone from small to high landslide probability in the two planes also confirms that the power-law equation (a straight line in a log-log plane) and the linear equation are suitable functional formats for the threshold lines in the (D, I) and (θ, H) planes, respectively.

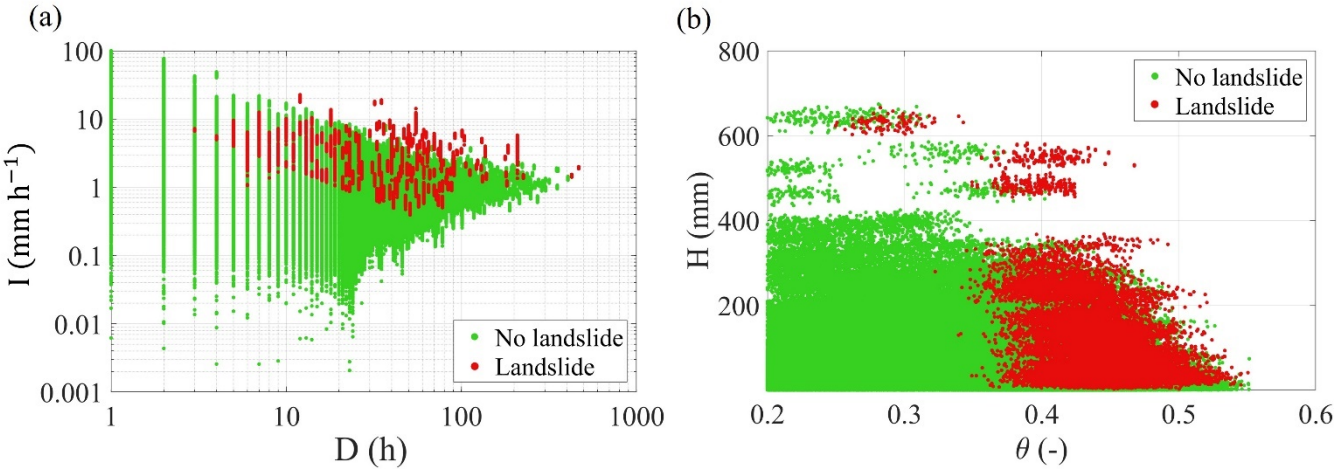

Figure 8. Scatter plot of perturbed meteorological and hydrometeorological variables of 100 scenarios: (a) in the meteorological plane (*D, I*) with logarithmic axes; (b) in the hydrometeorological plane (θ, *H*).

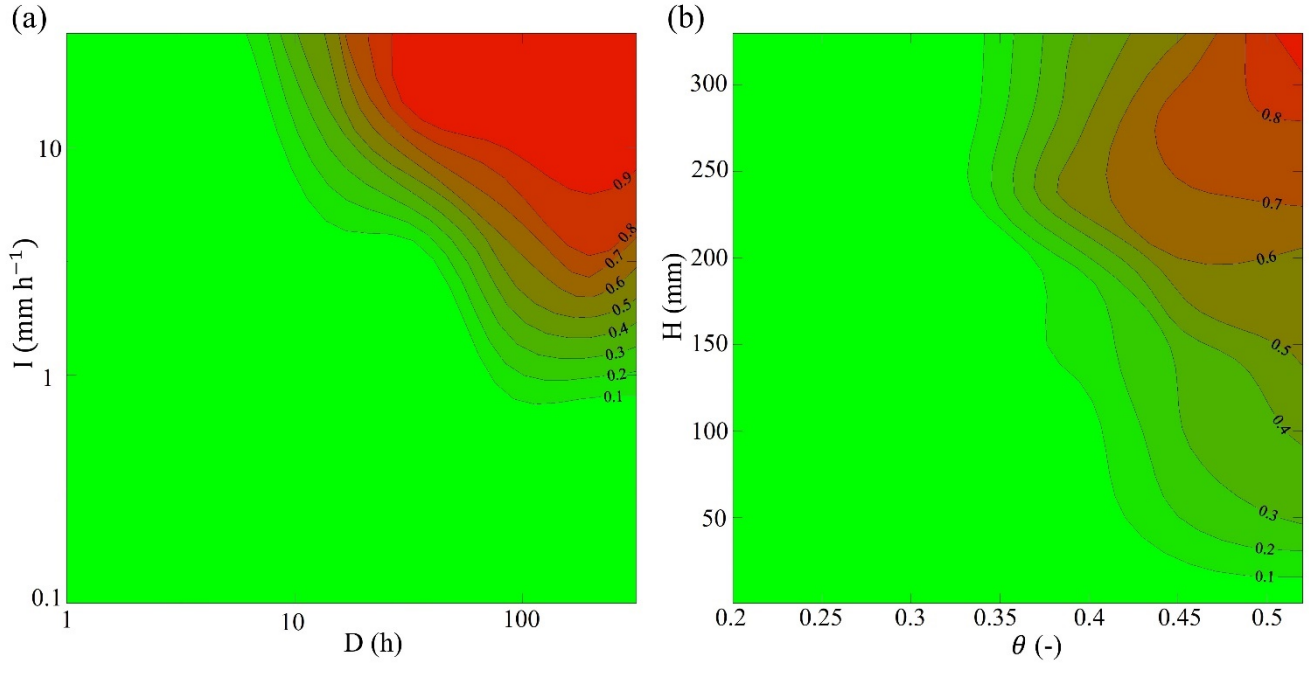

Figure 9. Conditional landslide probability distributions: (a) in the meteorological plane (D, I) with logarithmic axes; (b) in the hydrometeorological plane (θ, *H*).

https://doi.org/10.5194/egusphere-2024-2329
Preprint. Discussion started: 19 August 2024

The suitability of threshold lines has been investigated by defining an optimal threshold for each scenario (i.e., maximizing TSS), for all the functional formats tested for the reference slope.

Fig. 10 shows the scatter plot of the perturbed variables with the dashed thresholds obtained by calculating the mean value of threshold line parameters obtained for all scenarios, in the (D, I) plane with power-law equation (Fig. 10a), in the (θ, H) plane with linear equation (Fig. 10b), and in the 3D space (θ, h_a, H) with the bi-plane format (Figs. 10c and 10d). In the latter case, the events with landslides have been split in red and blue dots, according to the low and high-water level, respectively. Moreover, in Fig. 10, the shaded areas represent the spanning of the 100 thresholds obtained for all the scenarios.

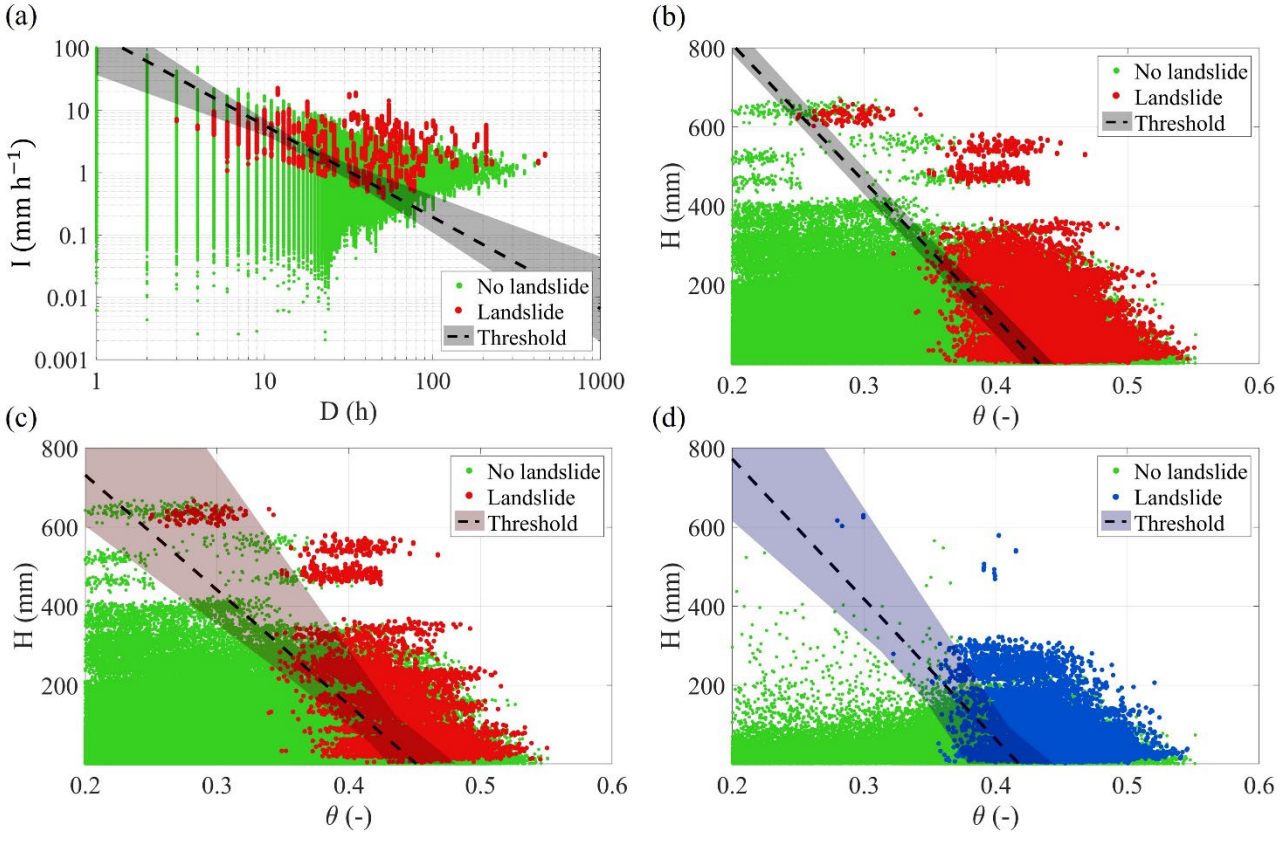

Figure 10. Scatter plot of perturbed meteorological and hydrometeorological variables with the thresholds obtained by the optimization of 100 scenarios using different functional formats: (a) Power-law meteorological thresholds in the meteorological plane (I, D) with logarithmic axes; (b) linear hydrometeorological thresholds in the plane (θ, H); Bi-plane hydrometeorological thresholds in the plane (θ, H) according to different antecedent aquifer level h_a: (c) low perched aquifer water level ($h_a \geq h_x$: red dots) and (d) high perched aquifer water level ($h_a < h_x$: blue dots).

The predictive performances displayed by the investigated thresholds for the large area (80 km^2) are consistent with those obtained for the reference slope. In fact, the performance increases moving from pure meteorological, to hydrometeorological

https://doi.org/10.5194/egusphere-2024-2329
Preprint. Discussion started: 19 August 2024

2D, to hydrometeorological 3D, as sketched in Fig. 11, in which the distributions of the obtained TSS values for all 100 scenarios are shown through box and whiskers plots.

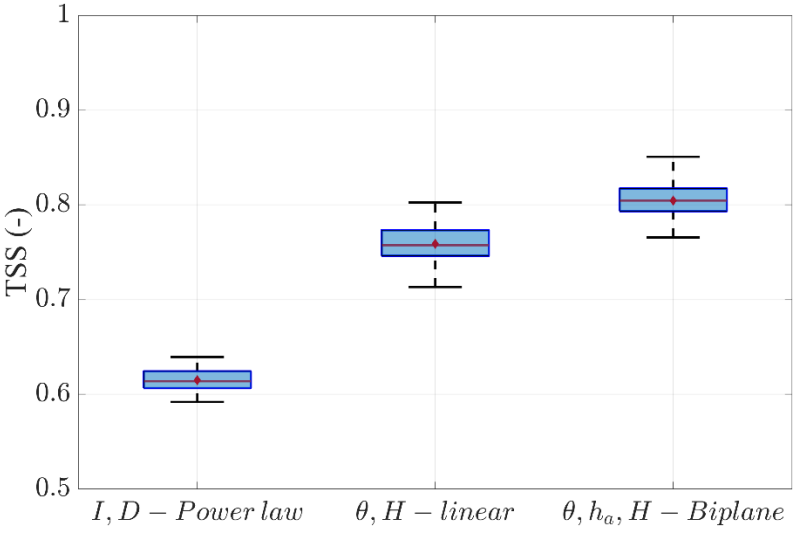

Figure 11. Performance comparison of the tested functional formats for all scenarios referred to meteorological and hydrometeorological thresholds.

As depicted in the box plots, the hydrometeorological approach leads to TSS values ranging between 0.72 and 0.80 (2D threshold), and between 0.77 and 0.85 (3D threshold). Instead, the meteorological approach shows TSS values between 0.59 and 0.64. For each functional format, the red lines inside the box represent the median value, overlapping with the average of TSS (red dots in the middle of the boxes). For the three tested formats, Table 7 summarizes the parameters and the performance indicators of the median TSS, as well as the overall TSS range (ΔTSS).

Table 7. Summary of performance indicators obtained by maximizing the TSS values of the landslide thresholds applied to the different scenarios.

Functional formats		a	b	h_x	TSS median	Missed alarms	False alarms	Total events	ΔTSS
Meteorological	Power-law	168.37	-1.47	-	0.614	26	6216	26363	0.05
Hydrometeorological	Linear	-3467.71	1502.54	-	0.757	16	3962		0.08
	Bi-plane	-2896.64	1308.85	11.03	0.804	11	3406		0.08
		-3559.64	1478.81						

Looking at 2D thresholds, the parameters of meteorological power-law exhibit a large change compared to one referred to reference slope (Table 5), likely due to the lack of physical basis, while the change for the simple linear hydrometeorological is less pronounced. However, looking at the 3D threshold, the change is more significant, owing to the addition of the random perturbation of groundwater level.

https://doi.org/10.5194/egusphere-2024-2329
Preprint. Discussion started: 19 August 2024

It is worth to note that the median linear hydrometeorological format allowed to obtain a total number of false alarms in the whole area equal to 3962 in 500 years (i.e., on average, 8 per year), with missed alarms only once every 31 years.
Moreover, applying the bi-plane threshold would further improve the predictive performance, leading to the lowest total number of missed alarms, i.e., only 11 in 500 years (on average once every 45 years), as well as the lowest number of false alarms, as reported in Table 7.

3.3 Application to real landslide dataset

A practical application to a real dataset has been carried out for the period from 2002 to 2020, during which 9 landslide events were registered and validated in the study area (Calvello and Pecoraro, 2018; Peruccacci et al., 2023). The rainfall time series within such temporal window has been taken from the Cervinara rain gauge station. For the root zone volumetric water content, θ, the ERA5 reanalysis data were used. The median 2D thresholds reported in Fig. 10 (section 3.2) have been kept for assessing their performances referred to the real landslide dataset. Figure 12a and 12b report, respectively, the application of the meteorological (D, I) and hydrometeorological (θ, H) thresholds.

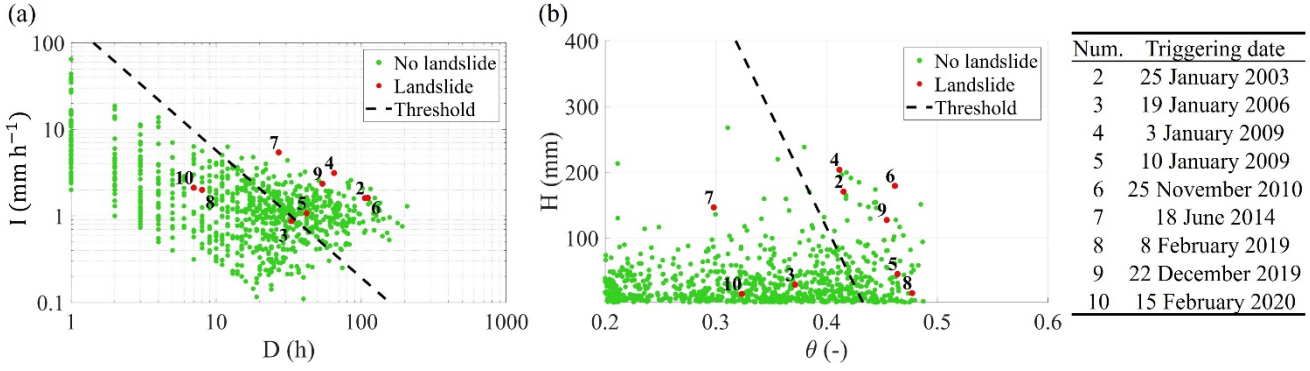

Num.	Triggering date
2	25 January 2003
3	19 January 2006
4	3 January 2009
5	10 January 2009
6	25 November 2010
7	18 June 2014
8	8 February 2019
9	22 December 2019
10	15 February 2020

Figure 12. Application to real landslides, from 2002 to 2020, of the power-law meteorological (a) and the linear hydrometeorological thresholds (b) defined in the section 3.2. In both planes, the scattered dots representing rainfall events not followed by any landslide (green dots) and rainfall events after which landslides were registered (red dots). On the right side, landslide triggering dates are reported.

Also in this case, the hydrometeorological threshold performs better in the prediction of real landslide occurrences. Indeed, it reaches a TSS value of 0.50, whereas for the purely meteorological it is equal only to 0.35. The number of false alarms results consistent with the application to the synthetic dataset (i.e., 143 and 269 in 19 years for the hydrometeorological and meteorological thresholds, respectively), but the missed alarms, three for both the thresholds, are much more than expected.
However, this result can be ascribed to intrinsic uncertainties affecting the landslide inventory, where indeed some of the reported landslides have been classified as having very limited geographic (i.e., landside nr. 3) or temporal (i.e., landside nr. 7) accuracy. Furthermore, the rain data from the gauge of Cervinara may be not representative for some of the farthest landslides (e.g., landslide nr. 10, represented in Fig. 1). The correction of just some of the three missed landslides would bring the performances back to the same level as for the synthetic dataset.

https://doi.org/10.5194/egusphere-2024-2329
Preprint. Discussion started: 19 August 2024

4 Conclusions

The paper investigates the potential advancements that may be achieved by including one or more hydrological variables in the definition of empirical thresholds for rainfall-induced landslide forecasting. As landslide inventories usually provide limited amounts of data suitable for statistical analyses, a 500-year long synthetic dataset has been generated by means of a physically based model. The model, previously calibrated and validated thanks to detailed laboratory and field experiments, reproduces the response to meteorological forcing of a reference slope, with perfectly known geomorphologic and physical properties. The reference slope is representative of a wide area of Campania (Italy), characterised by carbonate massifs covered with a thin layer of pyroclastic deposits, frequently affected by rainfall-induced shallow landslides.

The analysis of the synthetic dataset of the reference slope, including soil moisture and suction distributions in the soil deposit, as well as perched aquifer water level, allowed the assessment of slope stability at hourly resolution. The results show that a hydrometeorological threshold, based on root-zone soil moisture and rainfall depth, outperforms the usually adopted purely meteorological threshold, based on rainfall intensity and duration. Furthermore, a novel hydrometeorological threshold, defined in the 3D space of root-zone soil moisture and aquifer water level (as indicators of antecedent slope conditions) and rainfall depth, provides nearly unerring predictions of landslide triggering. The proposed 3D threshold also allows identifying the antecedent conditions leading to the activation of two different landslide triggering mechanisms, related to the beginning and the end of the rainy season.

To extend the analysis to a large area, the effects of the spatial variability of slope characteristics and rainfall has been introduced as Normal-distributed random perturbations of the reference slope variables. In fact, uncertainty affects the assessment of slope stability, as well as the representativeness for a wide area of hydrometeorological variables collected at few locations. The distributions of landslide probability, conditional to meteorological (i.e., rain intensity and duration) and hydrometeorological (i.e., root-zone soil moisture and rain depth) variables, clearly indicate that these latter are more robust with respect to uncertainty, as the transition from small to high landslide probability is sharper in the hydrometeorological plane. This result is confirmed by the small reduction of the predictive performance of the hydrometeorological thresholds applied at large scale, compared to the meteorological one.

The proposed approach, although based on synthetic data, looks promising for operational early warning application, as it is shown by the results obtained with real data for the north-facing side of Partenio Massif, with an extension of about 80 km^2. Specifically, rainfall data from a rain gauge of the area and root-zone soil moisture data from ERA5 meteorological reanalysis have been used to assess the performance of the obtained meteorological and hydrometeorological thresholds for the prediction of the landslides of the period 2002-2020 reported in available inventories. The small numbers of missed and false alarms indicate that the hydrometeorological threshold obtained with the synthetic data can be used as an effective tool for landslide early warning in the study area.

The obtained results point out the importance of supplementing meteorological networks with hydrological monitoring for landslide hazard assessment. In this respect, the possibility of getting information about perched aquifer level (e.g., linking it

https://doi.org/10.5194/egusphere-2024-2329
Preprint. Discussion started: 19 August 2024

to measurements of water level in supplied streams) should be investigated, as it would likely further improve the reliability of the predictions.

Data availability

All raw data can be provided by the corresponding author upon request.

Author contributions

All the authors designed the research; PM and GFS developed the model code and performed the simulations; AA, DCRQ and PM analyzed the data and plotted the graphs; RG supervised the study; PM and DCRQ wrote the manuscript draft; RG reviewed and edited the manuscript.

Competing interests

The authors declare that they have no conflict of interest.

Acknowledgements

This research is part of the Ph.D. project entitled “Hydrological controls and geotechnical features affecting the triggering of shallow landslides in pyroclastic soil deposits” within the Doctoral Course “A.D.I.” of Università degli Studi della Campania “L. Vanvitelli”.

The research has been also funded by the Politecnico di Milano in project entitled "Multi-Risk sciEnce for resilienT commUnities undeR a changiNg climate (RETURN)", PE00000005, SPOKE VS1, CUP D43C22003030002, within the National Recovery and Resilience Plan, granted by EU - NextGenerationEU.

References

Abraham, M. T., Satyam, N., Rosi, A., Pradhan, B., and Segoni, S.: Usage of antecedent soil moisture for improving the performance of rainfall thresholds for landslide early warning, Catena (Amst), 200, 105147, https://doi.org/10.1016/j.catena.2021.105147, 2021.

Autorità di Bacino: Mitigazione del rischio idrogeologico finalizzato al governo del territorio, Cervinara, Open File Rep. 1–82 pp., 2013.

Baum, R. L. and Godt, J. W.: Early warning of rainfall-induced shallow landslides and debris flows in the USA, Landslides, 7, 259–272, https://doi.org/10.1007/s10346-009-0177-0, 2010.

https://doi.org/10.5194/egusphere-2024-2329
Preprint. Discussion started: 19 August 2024

Beck, H. E., Pan, M., Miralles, D. G., Reichle, R. H., Dorigo, W. A., Hahn, S., Sheffield, J., Karthikeyan, L., Balsamo, G., Parinussa, R. M., van Dijk, A. I. J. M., Du, J., Kimball, J. S., Vergopolan, N., and Wood, E. F.: Evaluation of 18 satellite- And model-based soil moisture products using in situ measurements from 826 sensors, Hydrol Earth Syst Sci, 25, 17–40, https://doi.org/10.5194/HESS-25-17-2021, 2021.

Bennett, G., Van Camp, M., Shemsanga, C., Kervyn, M., and Walraevens, K.: Assessment of spatial and temporal variability of groundwater level in the aquifer system on the flanks of Mount Meru, Northern Tanzania, J Hydrol Reg Stud, 44, 101212, https://doi.org/10.1016/J.EJRH.2022.101212, 2022.

Bogaard, T. and Greco, R.: Invited perspectives: Hydrological perspectives on precipitation intensity-duration thresholds for landslide initiation: proposing hydro-meteorological thresholds, Natural Hazards and Earth System Sciences, 18, 31–39, https://doi.org/10.5194/nhess-18-31-2018, 2018.

Bogaard, T. A. and Greco, R.: Landslide hydrology: from hydrology to pore pressure, WIREs Water, 3, 439–459, https://doi.org/10.1002/wat2.1126, 2016.

Breznitz, S.: Cry Wolf: The Psychology of False Alarms., Lawrence Erlbaum Associates, Hillsdale, New Jersey London, 1984.

Calvello, M. and Pecoraro, G.: FraneItalia: a catalog of recent Italian landslides, Geoenvironmental Disasters, 5, 1–16, https://doi.org/10.1186/S40677-018-0105-5/FIGURES/11, 2018.

Cascini, L., Cuomo, S., and Guida, D.: Typical source areas of May 1998 flow-like mass movements in the Campania region, Southern Italy, Eng Geol, 96, https://doi.org/10.1016/j.enggeo.2007.10.003, 2008.

Comegna, L., Damiano, E., Greco, R., Guida, A., Olivares, L., and Picarelli, L.: Field hydrological monitoring of a sloping shallow pyroclastic deposit, Canadian Geotechnical Journal, 53, 1125–1137, https://doi.org/10.1139/cgj-2015-0344, 2016.

Cowpertwait, P. S. P., O'Connell, P. E., Metcalfe, A. V., and Mawdsley, J. A.: Stochastic point process modelling of rainfall. I. Single-site fitting and validation, J Hydrol (Amst), 175, 17–46, https://doi.org/10.1016/S0022-1694(96)80004-7, 1996.

Crosta, G. B. and Dal Negro, P.: Observations and modelling of soil slip-debris flow initiation processes in pyroclastic deposits: the Sarno 1998 event, Natural Hazards and Earth System Sciences, 3, 53–69, https://doi.org/10.5194/NHESS-3-53-2003, 2003.

Damiano, E. and Olivares, L.: The role of infiltration processes in steep slope stability of pyroclastic granular soils: laboratory and numerical investigation, Natural Hazards, 52, 329–350, https://doi.org/10.1007/s11069-009-9374-3, 2010.

Damiano, E., Olivares, L., and Picarelli, L.: Steep-slope monitoring in unsaturated pyroclastic soils, Eng Geol, 137–138, 1–12, https://doi.org/10.1016/j.enggeo.2012.03.002, 2012.

Dari, J., Morbidelli, R., Saltalippi, C., Massari, C., and Brocca, L.: Spatial-temporal variability of soil moisture: Addressing the monitoring at the catchment scale, J Hydrol (Amst), 570, 436–444, https://doi.org/10.1016/J.JHYDROL.2019.01.014, 2019.

Del Soldato, M., Pazzi, V., Segoni, S., De Vita, P., Tofani, V., and Moretti, S.: Spatial modeling of pyroclastic cover deposit thickness (depth to bedrock) in peri-volcanic areas of Campania (southern Italy), Earth Surf Process Landf, 43, 1757–1767, https://doi.org/10.1002/ESP.4350, 2018.

https://doi.org/10.5194/egusphere-2024-2329
Preprint. Discussion started: 19 August 2024

De Vita, P. and Nappi, M.: Regional distribution of ash-fall pyroclastic soils for landslide susceptibility assessment, Landslide Science and Practice: Spatial Analysis and Modelling, 3, 103–109, https://doi.org/10.1007/978-3-642-31310-3_15, 2013.

Di Crescenzo, G. and Santo, A.: Debris slides-rapid earth flows in the carbonate massifs of the Campania region (Southern Italy): Morphological and morphometric data for evaluating triggering susceptibility, Geomorphology, 66, 255–276, https://doi.org/10.1016/j.geomorph.2004.09.015, 2005.

Feddes, R. A., Kowalik, P., Kolinska-Malinka, K., and Zaradny, H.: Simulation of field water uptake by plants using a soil water dependent root extraction function, J Hydrol (Amst), 31, 13–26, https://doi.org/10.1016/0022-1694(76)90017-2, 1976.

Fiorillo, F., Guadagno, F., Aquino, S., and De Blasio, A.: The December 1999 Cervinara landslides: Further debris flows in the pyroclastic deposits of Campania (Southern Italy), Bulletin of Engineering Geology and the Environment, 60, 171-184, https://doi.org/10.1007/s100640000093, 2001.

Froude, M. J. and Petley, D. N.: Global fatal landslide occurrence from 2004 to 2016, Natural Hazards and Earth System Sciences, 18, 2161–2181, https://doi.org/10.5194/nhess-18-2161-2018, 2018.

Goldberg, D. E. and Holland, J. H.: Genetic Algorithms and Machine Learning, Mach Learn, 3, 95–99, https://doi.org/10.1023/A:1022602019183/METRICS, 1988.

Gonzalez, R. J., Giraldo, E. A., Aristizábal, E. G., and Marin, R. J.: Physically-based Model applied to Rainfall Thresholds for Shallow Landslides: Literature review, Revista de la Asociación Geológica Argentina, 80, 164–178, 2023.

Greco, R., Comegna, L., Damiano, E., Guida, A., Olivares, L., and Picarelli, L.: Hydrological modelling of a slope covered with shallow pyroclastic deposits from field monitoring data, Hydrol Earth Syst Sci, 17, 4001–4013, https://doi.org/10.5194/hess-17-4001-2013, 2013.

Greco, R., Comegna, L., Damiano, E., Guida, A., Olivares, L., and Picarelli, L.: Conceptual Hydrological Modeling of the Soil-bedrock Interface at the Bottom of the Pyroclastic Cover of Cervinara (Italy), Procedia Earth and Planetary Science, https://doi.org/10.1016/j.proeps.2014.06.007, 2014.

Greco, R., Marino, P., Santonastaso, G. F., and Damiano, E.: Interaction between Perched Epikarst Aquifer and Unsaturated Soil Cover in the Initiation of Shallow Landslides in Pyroclastic Soils, Water (Basel), 10, 948, https://doi.org/10.3390/w10070948, 2018.

Greco, R., Comegna, L., Damiano, E., Marino, P., Olivares, L., and Santonastaso, G. F.: Recurrent rainfall-induced landslides on the slopes with pyroclastic cover of Partenio Mountains (Campania, Italy): Comparison of 1999 and 2019 events, Eng Geol, 288, 106160, https://doi.org/10.1016/j.enggeo.2021.106160, 2021.

Guzzetti, F., Peruccacci, S., Rossi, M., and Stark, C. P.: Rainfall thresholds for the initiation of landslides in central and southern Europe, Meteorology and Atmospheric Physics, 98, 239-267, https://doi.org/10.1007/s00703-007-0262-7, 2007.

Guzzetti, F., Peruccacci, S., Rossi, M., and Stark, C. P.: The rainfall intensity–duration control of shallow landslides and debris flows: an update, Landslides, 5, 3–17, https://doi.org/10.1007/s10346-007-0112-1, 2008.

https://doi.org/10.5194/egusphere-2024-2329
Preprint. Discussion started: 19 August 2024

Hanson, C. L.: DISTRIBUTION AND STOCHASTIC GENERATION OF ANNUAL AND MONTHLY PRECIPITATION ON A MOUNTAINOUS WATERSHED IN SOUTHWEST IDAHO1, JAWRA Journal of the American Water Resources Association, 18, 875–883, https://doi.org/10.1111/J.1752-1688.1982.TB00085.X, 1982.

Hartmann, A., Goldscheider, N., Wagener, T., Lange, J., and Weiler, M.: Karst water resources in a changing world: Review of hydrological modeling approaches, Reviews of Geophysics, 52, 218–242, https://doi.org/10.1002/2013RG000443, 2014.

Hersbach, H., Bell, B., Berrisford, P., Hirahara, S., Horányi, A., Muñoz-Sabater, J., Nicolas, J., Peubey, C., Radu, R., Schepers, D., Simmons, A., Soci, C., Abdalla, S., Abellan, X., Balsamo, G., Bechtold, P., Biavati, G., Bidlot, J., Bonavita, M., De Chiara, G., Dahlgren, P., Dee, D., Diamantakis, M., Dragani, R., Flemming, J., Forbes, R., Fuentes, M., Geer, A., Haimberger, L., Healy, S., Hogan, R. J., Hólm, E., Janisková, M., Keeley, S., Laloyaux, P., Lopez, P., Lupu, C., Radnoti, G., de Rosnay, P., Rozum, I., Vamborg, F., Villaume, S., and Thépaut, J. N.: The ERA5 global reanalysis, Quarterly Journal of the Royal Meteorological Society, 146, 1999–2049, https://doi.org/10.1002/QJ.3803, 2020.

Illien, L., Andermann, C., Sens-Schönfelder, C., Cook, K. L., Baidya, K. P., Adhikari, L. B., and Hovius, N.: Subsurface Moisture Regulates Himalayan Groundwater Storage and Discharge, AGU Advances, 2, e2021AV000398, https://doi.org/10.1029/2021AV000398, 2021.

Keskin, M. E., Taylan, D., and Terzi, Ö.: Adaptive neural-based fuzzy inference system (ANFIS) approach for modelling hydrological time series, Hydrological Sciences Journal, 51, 588–598, https://doi.org/10.1623/HYSJ.51.4.588, 2006.

Lu, N. and Likos, W. J.: Suction stress characteristic curve for unsaturated soil, Journal of Geotechnical and Geoenvironmental Engineering, 132, 131-142, https://doi.org/10.1061/(ASCE)1090-0241(2006)132:2(131), 2006.

Marino, P., Comegna, L., Damiano, E., Olivares, L., and Greco, R.: Monitoring the Hydrological Balance of a Landslide-Prone Slope Covered by Pyroclastic Deposits over Limestone Fractured Bedrock, Water (Basel), 12, 3309, https://doi.org/10.3390/w12123309, 2020a.

Marino, P., Peres, D. J., Cancelliere, A., Greco, R., and Bogaard, T.: Soil moisture information can improve shallow landslide forecasting using the hydrometeorological threshold approach, Landslides, 17, 2041–2054, https://doi.org/10.1007/s10346-020-01420-8, 2020b.

Marino, P., Santonastaso, G. F., Fan, X., and Greco, R.: Prediction of shallow landslides in pyroclastic-covered slopes by coupled modeling of unsaturated and saturated groundwater flow, Landslides, 18, 31–41, https://doi.org/10.1007/s10346-020-01484-6, 2021.

Marino, P., Roman Quintero, D. C., Santonastaso, G. F., and Greco, R.: Prototype of an IoT-Based Low-Cost Sensor Network for the Hydrological Monitoring of Landslide-Prone Areas, Sensors, 23, https://doi.org/10.3390/s23042299, 2023.

Michele, C. De, Salvadori, G., Canossi, M., Petaccia, A., and Rosso, R.: Bivariate Statistical Approach to Check Adequacy of Dam Spillway, J Hydrol Eng, 10, 50–57, https://doi.org/10.1061/(ASCE)1084-0699(2005)10:1(50), 2005.

Mirus, B. B., Morphew, M. D., and Smith, J. B.: Developing hydro-meteorological thresholds for shallow landslide initiation and early warning, Water, 10, 1274, https://doi.org/10.3390/W10091274, 2018a.

https://doi.org/10.5194/egusphere-2024-2329
Preprint. Discussion started: 19 August 2024

Mirus, B. B., Becker, R. E., Baum, R. L., and Smith, J. B.: Integrating real-time subsurface hydrologic monitoring with empirical rainfall thresholds to improve landslide early warning, Landslides, 15, 1909–1919, https://doi.org/10.1007/s10346-018-0995-z, 2018b.

Mirus, B. B., Bogaard, T., Greco, R., and Stähli, M.: Invited Perspectives: Integrating hydrologic information into the next generation of landslide early warning systems, EGUsphere [preprint], 1–19, https://doi.org/10.5194/egusphere-2024-1219, 2024.

Mualem, Y.: Hysteretical models for prediction of the hydraulic conductivity of unsaturated porous media, Water Resour Res, 12, https://doi.org/10.1029/WR012i006p01248, 1976.

Muñoz-Sabater, J., Dutra, E., Agustí-Panareda, A., Albergel, C., Arduini, G., Balsamo, G., Boussetta, S., Choulga, M., Harrigan, S., Hersbach, H., Martens, B., Miralles, D. G., Piles, M., Rodríguez-Fernández, N. J., Zsoter, E., Buontempo, C., and Thépaut, J. N.: ERA5-Land: A state-of-the-art global reanalysis dataset for land applications, Earth Syst Sci Data, 13, 4349–4383, https://doi.org/10.5194/ESSD-13-4349-2021, 2021.

Olivares, L. and Picarelli, L.: Shallow flowslides triggered by intense rainfalls on natural slopes covered by loose unsaturated pyroclastic soils, Geotechnique, 53, 283-287, https://doi.org/10.1680/geot.2003.53.2.283, 2003.

Pagano, L., Picarelli, L., Rianna, G., and Urciuoli, G.: A simple numerical procedure for timely prediction of precipitation-induced landslides in unsaturated pyroclastic soils, Landslides, 7, 273-289, https://doi.org/10.1007/s10346-010-0216-x, 2010.

Palazzolo, N., Peres, D. J., Creaco, E., and Cancelliere, A.: Using principal component analysis to incorporate multi-layer soil moisture information in hydrometeorological thresholds for landslide prediction: an investigation based on ERA5-Land reanalysis data, Natural Hazards and Earth System Sciences, 23, 279–291, https://doi.org/10.5194/nhess-23-279-2023, 2023.

Peirce, C. S.: The numerical measure of the success of predictions, Science, 4, 453–454, https://doi.org/10.1126/SCIENCE.NS-4.93.453-A, 1884.

Peres, D. J. and Cancelliere, A.: Derivation and evaluation of landslide-triggering thresholds by a Monte Carlo approach, Hydrology and Earth System Sciences, 18, 4913–4931, https://doi.org/10.5194/hess-18-4913-2014, 2014.

Peres, D. J. and Cancelliere, A.: Comparing methods for determining landslide early warning thresholds: potential use of non-triggering rainfall for locations with scarce landslide data availability, Landslides, 18, 3135–3147, https://doi.org/10.1007/S10346-021-01704-7/FIGURES/13, 2021.

Peres, D. J., Cancelliere, A., Greco, R., and Bogaard, T. A.: Influence of uncertain identification of triggering rainfall on the assessment of landslide early warning thresholds, Natural Hazards and Earth System Sciences, 18, 633–646, https://doi.org/10.5194/NHESS-18-633-2018, 2018.

Peruccacci, S., Gariano, S. L., Melillo, M., Solimano, M., Guzzetti, F., and Brunetti, M. T.: The ITAlian rainfall-induced LandslIdes CAtalogue, an extensive and accurate spatio-temporal catalogue of rainfall-induced landslides in Italy, Earth Syst Sci Data, 15, 2863–2877, https://doi.org/10.5194/ESSD-15-2863-2023, 2023.

https://doi.org/10.5194/egusphere-2024-2329
Preprint. Discussion started: 19 August 2024

Pirone, M., Papa, R., Nicotera, M. V., and Urciuoli, G.: Soil water balance in an unsaturated pyroclastic slope for evaluation of soil hydraulic behaviour and boundary conditions, J Hydrol (Amst), 528, 63–83, https://doi.org/10.1016/j.jhydrol.2015.06.005, 2015.

Reder, A., Pagano, L., Picarelli, L., and Rianna, G.: The role of the lowermost boundary conditions in the hydrological response of shallow sloping covers, Landslides, 14, 861–873, https://doi.org/10.1007/s10346-016-0753-z, 2017.

Rodriguez-Iturbe, I., Febres De Power, B., and Valdes, J. B.: Rectangular pulses point process models for rainfall: analysis of empirical data, J Geophys Res, 92, 9645-9656, https://doi.org/10.1029/JD092iD08p09645, 1987.

Rolandi G., Petrosino P., and McGeehin J.: The interplinian activity at Somma-Vesuvius in the last 3500 years, J. Volcanol. Geotherm. Res., 82, 19-52, https://doi.org/10.1016/S0377-0273(97)00056-5, 1998.

Roman Quintero, D. C., Marino, P., Santonastaso, G. F., and Greco, R.: Understanding hydrologic controls of sloping soil response to precipitation through machine learning analysis applied to synthetic data, Hydrol Earth Syst Sci, 27, 4151–4172, https://doi.org/10.5194/HESS-27-4151-2023, 2023.

Roman Quintero, D. C., Damiano, E., Olivares, L., and Greco, R.: Mechanical and hydraulic properties of unsaturated layered pyroclastic ashes in landslide-prone areas of Campania (Italy), Bulletin of Engineering Geology and the Environment, 1, 1–16, https://doi.org/10.1007/S10064-024-03783-X, 2024.

Salas, J. D., Sveinsson, O. G., Lane, W. L., and Frevert, D. K.: Stochastic Streamflow Simulation Using SAMS-2003, Journal of Irrigation and Drainage Engineering, 132, 112–122, https://doi.org/10.1061/(ASCE)0733-9437(2006)132:2(112), 2006.

Segoni, S., Piciullo, L., and Gariano, S. L.: A review of the recent literature on rainfall thresholds for landslide occurrence, 1483–1501, https://doi.org/10.1007/s10346-018-0966-4, 2018.

Terzaghi, K.: Theoretical Soil Mechanics, John Wiley & Sons, Inc., Hoboken, NJ, USA, https://doi.org/10.1002/9780470172766, 1943.

Thomas, M. A., Collins, B. D., and Mirus, B. B.: Assessing the Feasibility of Satellite-Based Thresholds for Hydrologically Driven Landsliding, Water Resour Res, 55, 9006–9023, https://doi.org/10.1029/2019WR025577, 2019.

Wicki, A., Lehmann, P., Hauck, C., Seneviratne, S. I., Waldner, P., and Stähli, M.: Assessing the potential of soil moisture measurements for regional landslide early warning, Landslides, 17, 1881–1896, https://doi.org/10.1007/s10346-020-01400-y, 2020.

Williams, P. W.: The role of the epikarst in karst and cave hydrogeology: A review, Int J Speleol, 37, 1–10, https://doi.org/10.5038/1827-806X.37.1.1, 2008.